Effect of Strain on Room-Temperature Spin Transport in math xmlns="http://www.w3.org/1998/Math/MathML" display="inline" overflow="scroll">msub>mi>Si /mi>mrow>mn>0.1/mn>/mrow>/msub>msub>mi>Ge/mi >mrow>mn>0.9/mn>/mrow>/msub>/math>

T. Naito, M. Yamada, Y. Wagatsuma, K. Sawano, and K. Hamaya

Phys. Rev. Applied **18**, 024005 — Published 2 August 2022

DOI: 10.1103/PhysRevApplied.18.024005

Effect of Strain on Room-temperature Spin Transport in $Si_{0.1}Ge_{0.9}$

T. Naito,[1] M. Yamada,[2,3] Y. Wagatsuma,[4] K. Sawano,[4] and K. Hamaya[3,1,5a]

[1] *Department of Systems Innovation, Graduate School of Engineering Science, Osaka University, 1-3 Machikaneyama, Toyonaka 560-8531, Japan.*

[2] *PRESTO, Japan Science and Technology Agency, 4-1-8 Honcho, Kawaguchi, Saitama 332-0012, Japan.*

[3] *Center for Spintronics Research Network, Graduate School of Engineering Science, Osaka University, 1-3 Machikaneyama, Toyonaka 560-8531, Japan.*

[4] *Advanced Research Laboratories, Tokyo City University, 8-15-1 Todoroki, Tokyo 158-0082, Japan. and*

[5] *Spintronics Research Network Division, Institute for Open and Transdisciplinary Research Initiatives, Osaka University, Yamadaoka 2-1, Suita, Osaka, 565-0871, Japan.*

(Dated: July 7, 2022)

We report a strain effect on spin transport in semiconductors that exhibit Ge-like conduction bands at room temperature. Using four-terminal nonlocal spin-transport measurements in lateral spin-valve devices, we experimentally estimate the spin diffusion length (λ) of Ge and strained $Si_{0.1}Ge_{0.9}$ with two different carrier concentrations. Despite the Ge-like electronic band structure, the obtained λ of a strained $Si_{0.1}Ge_{0.9}$ is comparable to that of a Si channel. We discuss a possible mechanism of the strain-induced enhancement of λ at room temperature. As a consequence, we demonstrate the electrical detection of 5 μm lateral spin transport in the strained $Si_{0.1}Ge_{0.9}$ by applying an electric field at room temperature.

[a] E-mail: hamaya.kohei.es@osaka-u.ac.jp

I. INTRODUCTION

Lattice strain in semiconductors enables modification of their electronic band structure, including their bandgap, electronic charge density, and phonon frequency [1–6]. In particular, strained III–V and group-IV semiconductors have been widely investigated theoretically and experimentally because lattice strain can be applied in these materials through heterointerfaces formed via epitaxial growth techniques, leading to important advances in the field of condensed-matter physics and to various applications [7–14]. Recent studies of two-dimensional semiconductors have revealed a novel strain effect on the electronic band structures and bandgaps even in graphene [15, 16], transition-metal dichalcogenides [17, 18], and monolayer honeycomb elements [19–21].

Thus far, electron and hole mobility have been enhanced by in-plane biaxial or longitudinal uniaxial strain in group-IV channel layers [7–11]. For example in Ge(111), the in-plane biaxial and tensile strain causes energy splitting between a one-fold and three-fold L valleys in the conduction band, leading to electrons occupying a one-fold L valley with greater electron mobility [22–24]. In addition, the lattice strain in Ge induced by Si dramatically changes the physical properties because of the energy proximity ($\sim$ 140 meV) between the conduction-band minima at L points and the Γ point. Tensile strain is well known to decrease the energy difference between the L and Γ gaps, enhancing the optically accessible nature of Ge [25, 26]. Even for spins, Bottegoni *et al.* and Pezzoli *et al.* have reported on the high spin polarization and long spin lifetime in strained Ge layers or Ge quantum wells grown on SiGe [27–30], respectively, lifting the heavy hole–light hole degeneracy in the valence band of Ge. Recently, Cesari *et al.* [31] used strained Ge-rich $Ge_{1-x}Sn_x$ alloys to effectively explore spin-related optical properties.

Theoretical and experimental studies on the effect of strain on the spin relaxation mechanism in Si and/or Ge have also been reported. In particular, because the dominant spin relaxation pathway in Si and Ge is spin-flip scattering between the conduction-band valleys (i.e., intervalley spin-flip scattering) induced by electron–phonon [32–38] and electron–impurity interactions [39–41] through the spin–orbit coupling in host materials and impurities, respectively. Tang *et al.*, Li *et al.*, and Chalaev *et al.* have theoretically predicted suppression of intervalley spin-flip scattering through the strain, leading to lifting of the degenerate valleys at six Δ points for Si or at four L points for Ge [33, 35, 42]. Even in the case of pure spin current transport, the impurity-induced intervalley spin-flip scattering was partly suppressed at low temperatures when a strained heavily doped n-$Si_{0.1}Ge_{0.9}$(111) layer was used [43], where the Ge-rich $Si_{1-x}Ge_x$ exhibited a Ge-like electronic band structure with conduction-band minima at L points. However, because of the marked influences of electron–phonon interactions and experimental difficulties, it has been difficult to clarify the effect of the lattice strain on the spin transport in group IV semiconductors at room temperature.

Here we report a strain-induced enhancement in one of the spin-related physical properties, the spin diffusion length (λ), in a semiconductor at room temperature. Note that the difference in the band structure between $Si_{0.1}Ge_{0.9}$ and pure Ge is quite small [44, 45] and the position of the Fermi level (E_F) can easily be tuned by varying the doping concentration in the $Si_{0.1}Ge_{0.9}$ and pure Ge channel. Using four-terminal nonlocal spin-transport measurements in lateral spin-valve (LSV) devices, we clearly observe room-temperature spin transport in the strained $Si_{0.1}Ge_{0.9}$ and experimentally estimate the λ of the strained $Si_{0.1}Ge_{0.9}$. As a consequence, for an electron carrier concentration (n) of 1×10^{18} cm^{-3}, the λ of the strained $Si_{0.1}Ge_{0.9}$ is much larger than that of the pure Ge. Despite the Ge-like electronic band structure, the obtained λ of the strained $Si_{0.1}Ge_{0.9}$ is comparable to that of a Si channel at room temperature in Ref. [40]. We discuss a possible origin of the strain-induced enhancement of λ and demonstrate the electrical detection of 5 μm lateral spin transport in the strained $Si_{0.1}Ge_{0.9}$ by applying an electric field at room temperature.

II. RESULTS AND DISCUSSION

A. Growth and electrical properties of strained $Si_{0.1}Ge_{0.9}$

We prepare coherently grown Ge-rich $Si_{1-x}Ge_x$ ($Si_{0.1}Ge_{0.9}$) and Ge spin-transport layers on a Ge buffer layer on Si(111) substrate. Figure 1(a) shows a schematic and the nominal thicknesses of the n-$Si_{0.1}Ge_{0.9}$ spin-transport layer grown on a Ge buffer layer/Si(111). Here, the heterostructure was grown by molecular beam epitaxy (MBE) as follows. First, a Ge(111) buffer layer on an undoped Si(111) substrate ($\rho \sim 1000\ \Omega$ cm) was formed via a two-step growth method [46], where the first undoped Ge layer ($\sim$30 nm) was grown at 350 °C (LT-Ge), followed by an undoped Ge layer ($\sim$500 nm) grown at 700 °C (HT-Ge). The Ge buffer layer was relaxed, and misfit dislocations were confined near the Ge/Si(111) interface, as shown in Ref. [43]. On top of the HT-Ge layer, a 70 nm-thick phosphorus (P)-doped n-$Si_{0.1}Ge_{0.9}$(111) layer was grown by MBE at 350 °C [47]. Finally, a 7 nm-thick P δ-doped Ge layer with a 0.3 nm-thick Si layer was grown on top of the spin-transport layer for the Schottky tunnel conduction of electrons in spin-transport measurements [48]. As a reference, 140 nm-thick P-doped n-Ge(111) layers on an HT-Ge layer ($\sim$70 nm) [49] were also prepared to verify the strain effect. Figure 1(b) displays a two-dimensional X-ray diffraction (XRD) reciprocal space map for the grown $Si_{0.1}Ge_{0.9}$/Ge/Si(111) heterostructure, where Q_x and Q_z are

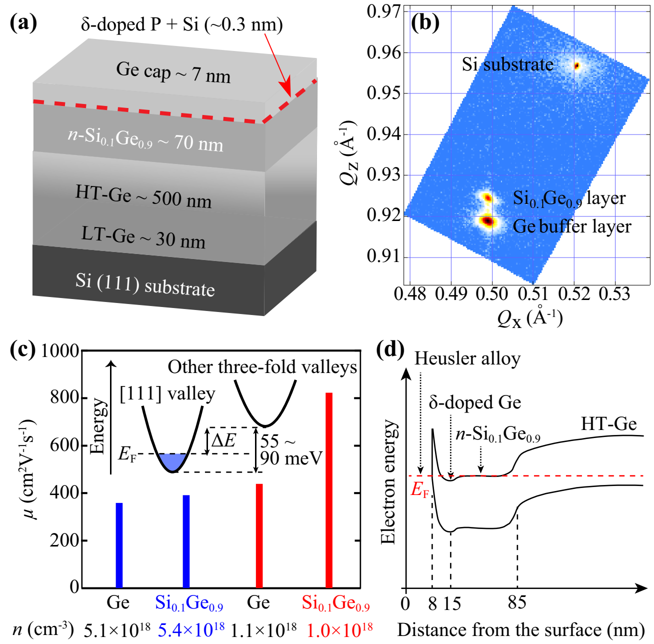

FIG. 1. (Color online) (a) Schematic of the grown n-$Si_{0.1}Ge_{0.9}$/Ge/Si(111) heterostructure for spin-transport measurements of the strained n-$Si_{0.1}Ge_{0.9}$. (b) Asymmetric (153) reciprocal space map of the $Si_{0.1}Ge_{0.9}$/Ge/Si(111). The $Si_{0.1}Ge_{0.9}$ layer is fully strained on the Ge buffer layer. (c) Electron Hall mobility of the strained n-$Si_{0.1}Ge_{0.9}$ and n-Ge with relatively high ($\sim 5\times10^{18}$ cm^{-3}) and low ($\sim 1\times10^{18}$ cm^{-3}) carrier concentrations at 300 K. The inset shows a schematic of the conduction-band valleys in the strained n-$Si_{0.1}Ge_{0.9}$. (d) Schematic of a band lineup of a part of the Co-based Heusler/P δ-doped Ge/n-$Si_{0.1}Ge_{0.9}$/HT-Ge (p-Ge).

the reciprocal space lattice parameters for in-plane and out-of-plane, respectively. Because of the difference in the lattice constant between Si and Ge, the (Q_x, Q_z) positions between the Si substrate and the grown Ge buffer layer differ dramatically. However, we observe matching of the Q_x parameter between the Ge buffer layer and the grown $Si_{0.1}Ge_{0.9}$ layer. This matching means that the grown $Si_{0.1}Ge_{0.9}$ layer on the Ge buffer layer is fully strained toward the layer plane, indicating biaxial tensile strain (ε_x) in (111). A comparison of the lattice constant of the strained $Si_{0.1}Ge_{0.9}$ and that reported for unstrained $Si_{0.1}Ge_{0.9}$ [50] indicates that the value of ε_x should be 0.64–0.66 %. Here we should also consider the presence of the tensile strain ($\varepsilon_x \sim 0.2$ %) in the Ge buffer layer from the Si substrate due to the mismatch in thermal expansion coefficients between Ge and Si. However, there was no impact on the electron Hall mobility and spin diffusion length at room temperature for the Ge spin-transport layers studied in the present study. Thus, in the strained $Si_{0.1}Ge_{0.9}$, we can simply predict that the four degenerate L valleys are lifted into a one-fold low-energy valley and three-fold higher-energy valleys [22–24, 33, 35], as depicted in the inset of Fig. 1(c).

To measure the electrical properties of the strained $Si_{0.1}Ge_{0.9}$ layer, we processed the heterostructure into Hall bar devices. From the longitudinal resistance (V_{xx}/I) and Hall voltage (V_{xy}) measurements, we determined the electrical resistivity (ρ) and electron carrier concentration (n) and estimated the electron mobility (μ) [Fig. 1(c)] at room temperature for the strained $Si_{0.1}Ge_{0.9}$ and Ge layers. By tuning the doping concentration of P in the channel layers, we prepared Ge and strained $Si_{0.1}Ge_{0.9}$ layers with two different n values: $\sim 5\times10^{18}$ cm^{-3} and $\sim 1\times10^{18}$ cm^{-3} [bottom of Fig. 1(c)]. Thus, in the present study, we compare these four channels to clarify the strain effect on room-temperature spin transport in semiconductors. Here the HT-Ge layer is undoped but exhibits p-type conduction due to the defect-induced hole generation [46], leading to the formation of a p-n junction at the n-SiGe/HT-Ge heterointerface [Fig. 1(d)]. As a result, the electron spin diffusion toward the Ge-on-Si substrate can be suppressed. Importantly, the strained $Si_{0.1}Ge_{0.9}$ layer with $n \sim 1\times10^{18}$ cm^{-3} clearly shows an almost twofold enhancement in μ at room temperature. This enhancement is consistent with the increase in the population of conduction electrons in the lowest L valley, which has a relatively small electron effective mass compared with the other three valleys [22–24]. On the basis of the literature [51, 52], the energy splitting of the conduction L valleys for the strained $Si_{0.1}Ge_{0.9}$ is theoretically expected to be 55–90 meV.

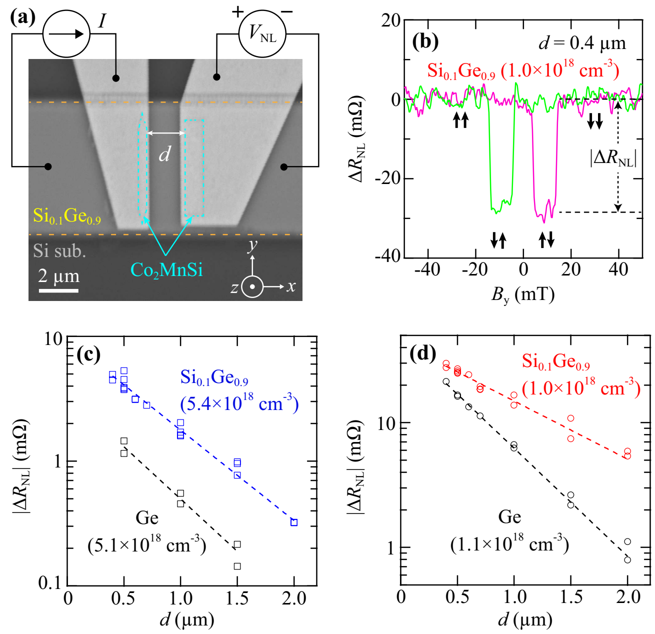

FIG. 2. (Color online) (a) Scanning electron microscopy (SEM) image of a lateral spin-valve (LSV) device fabricated using the strained n-$Si_{0.1}Ge_{0.9}$. (b) A nonlocal spin signal for the strained $Si_{0.1}Ge_{0.9}$ with $n \sim 1.0\times10^{18}$ cm^{-3} at $d = 0.4$ μm and at room temperature. (c) and (d) show the d-dependence of $|\Delta R_{NL}|$ at room temperature for $Si_{0.1}Ge_{0.9}$ and Ge with two different n values of $\sim5\times10^{18}$ cm^{-3} and $\sim1\times10^{18}$ cm^{-3}, respectively. The linear fits to the data using Eq. (1) are represented as dashed lines.

B. Spin transport in strained $Si_{0.1}Ge_{0.9}$

To examine the spin transport in semiconductors, we focused on four-terminal nonlocal voltage measurements in LSV devices [53, 54]. The top view of a fabricated LSV device with the strained n-$Si_{0.1}Ge_{0.9}$ channel layer is shown in Fig. 2(a), where d is the edge-to-edge distance between the spin injector and the detector. The size of the spin injector (detector) contact is 0.4×5.0 μm^2 (1.0×5.0 μm^2). Details of the fabrication processes and top views of similar LSV devices have been reported elsewhere [48, 55]. As the spin injector and detector materials, we used Co-based Heusler alloys [56, 57] such as $Co_2FeAl_{0.5}Si_{0.5}$ and Co_2MnSi, which were grown by MBE on top of the Schottky tunnel barriers [48, 58]. Here, a 0.7 nm-thick Fe layer was inserted between the Co-based Heusler alloy and the Ge cap layer to obtain large spin signals at room temperature [59, 60]. All the measurements were carried out at room temperature ($\sim$ 298 K) by applying a negative direct current ($I < 0$), for which the spin-polarized electrons were injected into the semiconductor channel used here, under applied in-plane (B_y) or out-of-plane (B_z) magnetic fields.

Figure 2(b) shows a representative nonlocal spin signal $[\Delta R_{NL} = \Delta V_{NL}/I = (V_{NL}^{\uparrow\downarrow} - V_{NL}^{\uparrow\uparrow})/I]$ as a function of B_y for an LSV device ($d = 0.4$ μm) with the strained n-$Si_{0.1}Ge_{0.9}$ with $n \sim 1.0 \times10^{18}$ cm^{-3}. Hysteretic behavior depending on the magnetization switching between the parallel and antiparallel states is clearly observed at room temperature. Here, the magnitude of ΔR_{NL}, $|\Delta R_{NL}|$, can be determined as described in Fig. 2(b). To estimate λ, we plot $|\Delta R_{NL}|$ as a function of d for the strained $Si_{0.1}Ge_{0.9}$ and Ge LSV devices with $n \sim 5 \times10^{18}$ cm^{-3} and $n \sim 1 \times10^{18}$ cm^{-3} in Figs. 2(c) and 2(d), respectively. For all the four-channel LSV devices, $|\Delta R_{NL}|$ is found to decay exponentially with increasing d.

In general, the reduction in $|\Delta R_{NL}|$ with increasing d can be represented by the following equation [48, 53, 54],

$$|\Delta R_{NL}| = P^2 \frac{\rho\lambda}{S} \exp\left(-d/\lambda\right), \tag{1}$$

where P is the average of the spin injection and detection efficiency and S is the cross-sectional area of the semiconductor channels ($\sim$0.49 μm^2 for n-$Si_{0.1}Ge_{0.9}$ and $\sim$0.98 μm^2 for n-Ge). Here, we used the estimated ρ values of $\sim$7.5 and $\sim$3.0 mΩ cm for the strained n-$Si_{0.1}Ge_{0.9}$ with $n \sim 1.0 \times10^{18}$ cm^{-3} and $\sim 5.4 \times10^{18}$ cm^{-3}, respectively; by contrast, for the Ge with $n \sim 1.1 \times10^{18}$ cm^{-3} and $\sim 5.1 \times10^{18}$ cm^{-3}, we used the ρ values of $\sim$13.3 and $\sim$3.4 mΩ cm, respectively. As shown by the dashed curves in Figs. 2(c) and 2(d), all the decay behaviors can be fitted using

TABLE I. Spin diffusion length (λ), diffusion constant (D), and spin lifetime (τ) at room temperature for various semiconductor channels.

Channel	n (cm^{-3})	λ (μm)	D (cm^2/s)	τ (ns)
$Si_{0.1}Ge_{0.9}$	1.0 $\times10^{18}$	0.93	32	0.27
Ge	1.1 $\times10^{18}$	0.50	17	0.15
$Si_{0.1}Ge_{0.9}$	5.4 $\times10^{18}$	0.60	23	0.16
Ge	5.1 $\times10^{18}$	0.52	21	0.13
Si [40]	1.6 $\times10^{19}$	0.95	4.4	2.1

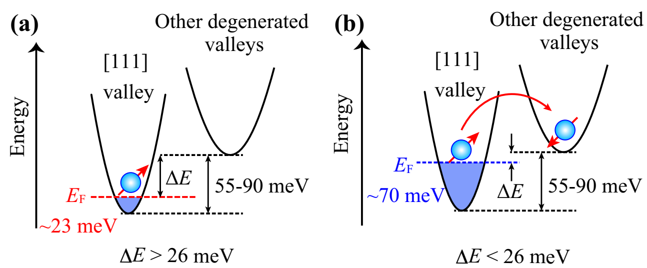

FIG. 3. (Color online) Schematics of the conduction-band valleys in the strained n-$Si_{0.1}Ge_{0.9}$ with (a) $n \sim 1{\times}10^{18}$ cm^{-3} and (b) $n \sim 5{\times}10^{18}$ cm^{-3} at room temperature.

Eq. (1), leading to the estimate of λ. Notably, the slope of the dashed curves for the strained n-$Si_{0.1}Ge_{0.9}$ is smaller than that for the Ge in both Figs. 2(c) and 2(d).

Table I shows a summary of the estimated λ values at room temperature for all four channels, together with the value for heavily doped Si [40]. The largest λ of 0.93 μm is obtained for the strained $Si_{0.1}Ge_{0.9}$ with $n \sim 1\times10^{18}$ cm^{-3}. Notably, the λ of 0.93 μm is large compared with that for the Ge ($n \sim 1\times10^{18}$ cm^{-3}). In addition, even for the SiGe channel with a Ge-like electronic band structure, the value of 0.93 μm for the strained $Si_{0.1}Ge_{0.9}$ is comparable to that ($\sim$ 0.95 μm [40]) for a Si channel with $n \sim 1.6\times10^{19}$ cm^{-3}. This means that the lattice strain enhances the electron spin diffusion length in a semiconductor channel.

To elucidate the mechanism of the marked enhancement in λ in the strained n-$Si_{0.1}Ge_{0.9}$ even at room temperature, we further estimate the spin lifetime (τ) using the relation $\lambda = \sqrt{D\tau}$, where D is the diffusion constant. In the present study, the value of D is determined from the modified Einstein's relation in Eq. (4) in Ref. [61] and the experimentally obtained n and μ in Fig. 1(c). The largest D of $\sim$32 cm^2/s is obtained for the strained n-$Si_{0.1}Ge_{0.9}$ with $n \sim 1\times10^{18}$ cm^{-3}, which is already expected from its largest electron mobility in Fig. 1(c). In addition to the D, the calculated τ for all four channels are also shown in Table I. The longest τ of $\sim$0.27 ns is also obtained for the strained n-$Si_{0.1}Ge_{0.9}$ with $n \sim 1\times10^{18}$ cm^{-3}. This feature indicates that suppression of an electron spin relaxation becomes evident in the strained n-$Si_{0.1}Ge_{0.9}$ with $n \sim 1\times10^{18}$ cm^{-3}. From the above, we conclude the enhancement in λ attributes not only to the enhancement in D but to the enhancement in τ. We also find almost no difference in τ between the Ge with $n \sim 1\times10^{18}$ cm^{-3} and that with $n \sim 5\times10^{18}$ cm^{-3}. Thus, for Ge at room temperature, the phonon-induced spin relaxation is dominant rather than the donor-driven spin relaxation [43].

A simple picture of the suppression mechanism of spin relaxation is drawn in Fig. 3. Here the Fermi level (E_F) above the conduction band edge was roughly estimated as $\hbar^2(3\pi^2 n)^{2/3}/(2m_e)$ and the valley energy splitting (55 – 90 meV) after applying a biaxial tensile strain in (111) to a Ge-like conduction band was also shown by referring to the literature [51, 52]. Figures 3(a) and 3(b) show schematics of the correlation between the valley energy splitting and E_F for the strained n-$Si_{0.1}Ge_{0.9}$ with $n \sim 1\times10^{18}$ cm^{-3} and $n \sim 5\times10^{18}$ cm^{-3}, respectively. In both cases, we concentrate on the energy difference (ΔE) between the valley energy splitting and E_F. When the ΔE is greater than approximately 26 meV (300 K), the phonon-induced spin-flip scattering between valleys can be suppressed even at room temperature [Fig. 3(a)]. On the other hand, if the ΔE becomes less than approximately 26 meV, phonon-induced intervalley scattering can occur frequently [Fig. 3(b)]. Thus, in addition to the formation of the valley energy splitting, the position of the E_F should be considered when a semiconductor channel is designed as a room-temperature spin-transport layer.

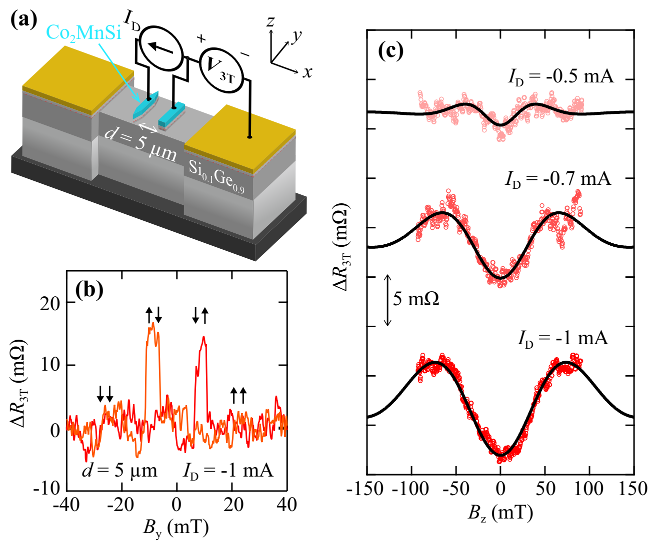

FIG. 4. (Color online) (a) Schematic of an LSV device fabricated using the strained n-$Si_{0.1}Ge_{0.9}$ ($n \sim 1.0\ \times 10^{18}$ cm^{-3}) for three-terminal nonlocal spin-transport measurements. (b) Three-terminal nonlocal spin signal at $d = 5$ μm, at $I_{\rm D} = -1$ mA, and at room temperature. (c) Hanle precession signals in a parallel magnetization state at $d = 5$ μm, at various $I_{\rm D}$ of -0.5, -0.7, and -1 mA, and at room temperature. The solid curves are curves simulated using Eq. (2).

C. Spin drift in strained $Si_{0.1}Ge_{0.9}$

Until now, long-distance spin transport in semiconductors such as Si [62–65] and Ge [37] has been electrically detected by a method using a spin drift effect. However, for Ge-like conduction-band channels, no study of the electrical detection of the long-distance spin transport at room temperature has been reported. Thus, we here explore the effect of strain on the long-distance spin transport in LSV devices at room temperature. For the strained n-$Si_{0.1}Ge_{0.9}$ with $n \sim 1.0\ \times 10^{18}$ cm^{-3}, we measure three-terminal nonlocal spin signals detected in the terminal configuration depicted in Fig. 4(a), where a negative direct current ($I_{\rm D} < 0$) is applied between the spin injector and the detector contacts [64, 66]. Figure 4(b) shows the room-temperature three-terminal nonlocal spin signal [$\Delta R_{\rm 3T} = \Delta V_{\rm 3T}/I_{\rm D} = (V_{\rm 3T}^{\uparrow\downarrow} - V_{\rm 3T}^{\uparrow\uparrow})/I_{\rm D}$] as a function of $B_{\rm y}$ at $d = 5$ μm and at $I_{\rm D} = -1$ mA. Despite the Ge-like conduction channel, a lateral spin transport of 5 μm is electrically detected in an LSV device with the strained $Si_{0.1}Ge_{0.9}$ at room temperature unlike its optical detection [67, 68]. By applying out-of-plane magnetic fields ($B_{\rm z}$), we also observe Hanle precession signals in a parallel magnetization state at various $I_{\rm D}$ in Fig. 4(c). The solid curves are simulated curves based on the following equation [53, 54]:

$$\Delta R(B_{\rm z}) = \pm \frac{P^2 \rho D}{S} \int_0^\infty \frac{1}{\sqrt{4\pi D t}} \exp\left[-\frac{(l - \nu_{\rm d} t)^2}{4Dt}\right] \times \cos\left(\frac{g\mu_{\rm B} B_{\rm z}}{\hbar} t\right) \exp\left(-\frac{t}{\tau}\right) dt, \tag{2}$$

where $D = 32$ cm^2/s and $\tau = 0.27$ ns are fixed to the values in Table I, the center-to-center distance (l) between the spin injector and detector contacts is 5.45 μm (corresponding to the edge-to-edge distance d of 5 μm), $\rho = 7.5$ mΩ cm, and the drift velocity ($\nu_{\rm d}$) is the product of the mobility $\mu = 823$ cm^2/(V s) in Fig. 1(c). The electron g-factor (g) is set as a free parameter and is roughly estimated to be $1.13 - 1.47$, which falls in the range from 0.82 (electrons populate only in the lower energy L valley) to 1.56 (electrons populate equally in the four L valleys) [52]. When the values of P, which only affect the amplitude of the Hanle curves, are selected to be 1.61, 2.38, and 2.55 % for $I_{\rm D}$ $= -0.5$, -0.7, and -1 mA, respectively, the simulated curves show good agreement with the experimental results. Notably, the difference in the P values among various $I_{\rm D}$ originates mainly from an enhancement in the spin detection efficiency at a biased Schottky-tunnel contact [66]. These results indicate that the experimentally obtained λ, D, and τ are valid physical quantities for the strained $Si_{0.1}Ge_{0.9}$ with $n \sim 1.0\ \times 10^{18}$ cm^{-3}.

To confirm the effect of electric fields (E) on the long-distance spin transport in the strained $Si_{0.1}Ge_{0.9}$, we finally examine the exponential decay behavior of $\Delta R_{\rm 3T}$ with varying d and $I_{\rm D}$ at room temperature, where the value of $I_{\rm D}$

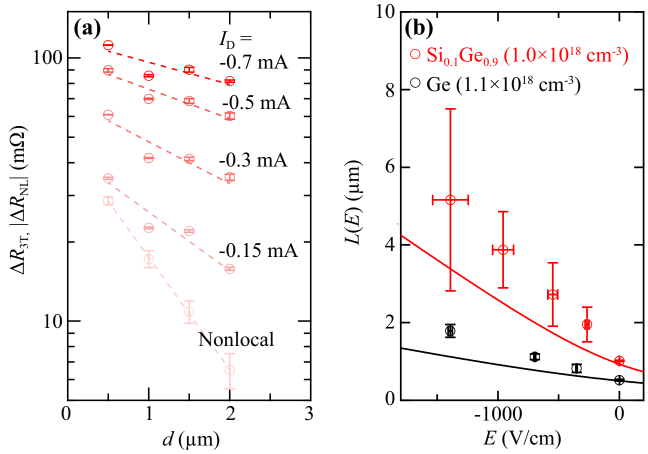

FIG. 5. (Color online) (a) d-dependence of ΔR_{3T} at room temperature for the strained $Si_{0.1}Ge_{0.9}$ with $n \sim 1\times10^{18}$ cm^{-3}, together with $|\Delta R_{NL}|$. The linear fits to the data using $\Delta R_{3T} \propto \exp(-d/L)$ are represented as dashed lines. (b) Room-temperature spin-transport length $L(E)$ as a function of E for $Si_{0.1}Ge_{0.9}$ (red) and Ge (black) with $n \sim 1\times10^{18}$ cm^{-3}. The solid curves are simulated data for $Si_{0.1}Ge_{0.9}$ (red) and Ge (black) with $\lambda = 0.93$ and 0.50 μm, respectively.

is related to that of E in the three-terminal nonlocal measurements in Fig. 4(a). Figure 5(a) shows the d-dependence of ΔR_{3T} with varying I_D in an LSV device with the strained $Si_{0.1}Ge_{0.9}$ with $n \sim 1\times10^{18}$ cm^{-3} at room temperature, together with the d-dependence of $|\Delta R_{NL}|$ in the same LSV device. We clearly observe that the exponential decay behavior of ΔR_{3T} becomes evidently moderate when I_D is increased. The dashed lines are linear fits to the data using $\Delta R_{3T} \propto \exp(-d/L)$ at a certain I_D, where L is the spin-transport length. Thus, we can estimate L from the fitting for various E. Figure 5(b) displays plots of L versus E for the strained $Si_{0.1}Ge_{0.9}$ (red) and the pure Ge (black) at room temperature. The estimated L for the strained $Si_{0.1}Ge_{0.9}$ is substantially enhanced with increasing $|E|$ compared to that for the pure Ge.

If E is applied to the spin-transport semiconductor channels, the value of L can become a function of E using the following equation [69–71]:

$$L(E) = \left(\frac{eE}{2\varepsilon_d} + \sqrt{\left(\frac{eE}{2\varepsilon_d}\right)^2 + \left(\frac{1}{\lambda}\right)^2} \right)^{-1}, \tag{3}$$

where e is the elementary charge and ε_d $(= eD/\mu)$ is an energy scale that controls the strength of the spin drift. Thus, we can simulate L as a function of E using Eq. (3). In the same panel of Fig. 5(b), the calculated $L(E)$ as a function of E using Eq. (3) is depicted, where $\varepsilon_d = 39$ meV and $\lambda = 0.93$ μm for the strained $Si_{0.1}Ge_{0.9}$ and $\varepsilon_d = 39$ meV and $\lambda = 0.50$ μm for the Ge are used. Although slight differences between the experimental data and the calculated ones are seen, the strain-induced enhancement in L is roughly reproduced using the enhancement in λ in Eq. (3). Thus, the long-distance spin transport in the strained n-$Si_{0.1}Ge_{0.9}$ ($n \sim 1.0 \times10^{18}$ cm^{-3}) in Fig. 4 is attributed to the strain-induced enhancement in $L(E)$ at room temperature even in Ge-like conduction-band channels. Therefore, understanding the effect of strain on the spin transport in semiconductors is important to the development of semiconductor spintronic applications at room temperature.

III. CONCLUSION

The effect of lattice strain on the spin transport in semiconductors is studied using four-terminal nonlocal spin-transport measurements in LSV devices with various semiconductor channels with Ge-like conduction bands. For $n = 1 \times10^{18}$ cm^{-3}, the λ of the strained $Si_{0.1}Ge_{0.9}$ is much larger than that of the pure Ge at room temperature. A possible mechanism of the strain-induced enhancement of λ is discussed as a consequence of a sufficient energy difference between the conduction valley splitting and E_F at room temperature. Because of the enhancement in λ and L by the strain, 5 μm lateral spin transport at room temperature is electrically detected by applying an electric field to the channel in an LSV device.

IV. ACKNOWLEDGMENTS

This work was supported in part by JSPS KAKENHI (Grant No. 19H05616, 19H02175, 21H05000), JST PRESTO (Grant No. JPMJPR20BA), and the Spintronics Research Network of Japan (Spin-RNJ). T.N. acknowledges JSPS Research Fellowship for Young Scientists (Grant No. 21J20019).

REFERENCES

---

[1] F. Cerdeira, C. J. Buchenauer, F. H. Pollak, and M. Cardona, Stress-Induced Shifts of First-Order Raman Frequencies of Diamond- and Zinc-Blende-Type Semiconductors, Phys. Rev. B **5**, 580 (1972).

[2] O. H. Nielsen and R. M. Martin, Stresses in semiconductors: *Ab initio* calculations on Si, Ge, and GaAs, Phys. Rev. B **32**, 3792 (1985).

[3] C. G. Van de Walle, Band lineups and deformation potentials in the model-solid theory, Phys. Rev. B **39**, 1871 (1989).

[4] M. V. Fischetti, and S. E. Laux, Band structure, deformation potentials, and carrier mobility in strained Si, Ge, and SiGe alloys, J. Appl. Phys. **80**, 2234 (1996).

[5] S. Poncé, D. Jena, and F. Giustino, Hole mobility of strained GaN from first principles, Phys. Rev. B **100**, 085204 (2019).

[6] Q. M. Thai, J. Chretien, M. Bertrand, L. Casiez, A. Chelnokov, V. Reboud, N. Pauc, and V. Calvo, GeSn optical gain and lasing characteristics modelling, Phys. Rev. B **102**, 155203 (2020).

[7] S. Takagi, J. L. Hoyt, J. J. Welser, and J. F. Gibbons, Comparative study of phonon-limited mobility of two-dimensional electrons in strained and unstrained Si metal-oxide-semiconductor field-effect transistors, J. Appl. Phys. **80**, 1567 (1996).

[8] M. L. Lee, E. A. Fitzgerald, M. T. Bulsara, M. T. Currie, and A. Lochtefeld, Strained Si, SiGe, and Ge channels for high-mobility metal-oxide-semiconductor field-effect transistors, J. Appl. Phys. **97**, 011101 (2005).

[9] Y. Sun, S. E. Thompson, and T. Nishida, Physics of strain effects in semiconductors and metal-oxide-semiconductor field-effect transistors, J. Appl. Phys. **101**, 104503 (2007).

[10] T. B. Boykin, M. Luisier, M. Salmani-Jelodar, and G. Klimeck, Strain-induced, off-diagonal, same-atom parameters in empirical tight-binding theory suitable for [110] uniaxial strain applied to a silicon parametrization, Phys. Rev. B **81**, 125202 (2010).

[11] Y. Chuang, C.-Y. Liu, G.-L. Luo, and J.-Y. Li, Electron Mobility Enhancement in GeSn n-Channel MOSFETs by Tensile Strain, IEEE Electron Device Lett. **42**, 10 (2021).

[12] G. C. Osbourn, $In_xGa_{1-x}As$–$In_yGa_{1-y}As$ strained-layer superlattices: A proposal for useful, new electronic materials, Phys. Rev. B **27**, 5126 (1983).

[13] C. Kisielowski, J. Krüger, S. Ruvimov, T. Suski, J. W. Ager, E. Jones, Z. Liliental-Weber, M. Rubin, E. R. Weber, M. D. Bremser, and R. F. Davis, Strain-related phenomena in GaN thin films, Phys. Rev. B **54**, 17745 (1996).

[14] S. Assali, A. Dijkstra, A. Attiaoui, É. Bouthillier, J. E. M. Haverkort, and O. Moutanabbir, Midinfrared Emission and Absorption in Strained and Relaxed Direct-Band-Gap $Ge_{1-x}Sn_x$ Semiconductors, Phys. Rev. Applied **15**, 024031 (2021).

[15] G. Gui, J. Li, and J. Zhong, Band structure engineering of graphene by strain: First-principles calculations, Phys. Rev. B **78**, 075435 (2008).

[16] Z. Gong, X. Shi, J. Li, S. Li, C. He, T. Ouyang, C. Zhang, C. Tang, and J. Zhong, Theoretical prediction of low-energy Stone-Wales graphene with an intrinsic type-III Dirac cone, Phys. Rev. B **101**, 155427 (2020).

[17] W. S. Yun, S. W. Han, S. C. Hong, I. G. Kim, and J. D. Lee, Thickness and strain effects on electronic structures of transition metal dichalcogenides: 2H-MX_2 semiconductors (M = Mo, W; X = S, Se, Te), Phys. Rev. B **85**, 033305 (2012).

[18] O. B. Aslan, M. Deng, M. L. Brongersma, and T. F. Heinz, Strained bilayer WSe_2 with reduced exciton-phonon coupling, Phys. Rev. B **101**, 115305 (2020).

[19] S. Zhang, Z. Yan, Y. Li, Z. Chen, and H. Zeng, Atomically Thin Arsenene and Antimonene: Semimetal–Semiconductor and Indirect–Direct Band-Gap Transitions, Angew. Chem. Int. Ed. **54**, 3112 (2015).

[20] Y. Li, H. B. Zhu, G. Q. Wang, Y. Z. Peng, J. R. Xu, Z. H. Qian, R. Bai, G. H. Zhou, C. Yesilyurt, Z. B. Siu, and M. B. A. Jalil, Strain-controlled valley and spin separation in silicene heterojunctions, Phys. Rev. B **97**, 085427 (2018).

[21] C. Kamal, Massless Dirac fermions in stable two-dimensional carbon-arsenic monolayer, Phys. Rev. B **100**, 205404 (2019).

[22] Y.-J. Yang, W. S. Ho, C.-F. Huang, S. T. Chang, and C. W. Liu, Electron mobility enhancement in strained-germanium n-channel metal-oxide-semiconductor field-effect transistors, Appl. Phys. Lett. **91**, 102103 (2007).

[23] M. Ono and T. Tezuka, Comprehensive Study of Electron Mobility and Band Gap in Tensile-Strained Bulk Ge, Jpn. J. Appl. Phys. **49**, 04DC20 (2010).

[24] F. Murphy-Armando, and S. Fahy, First principles calculation of electron-phonon and alloy scattering in strained SiGe, J. Appl. Phys. **110**, 123706 (2011).

[25] J. Liu, X. Sun, D. Pan, X. Wang, L. C. Kimerling, T. L. Koch, and J. Michel, Tensile-strained, n-type Ge as a gain medium for monolithic laser integration on Si, Optics Express **15**, 11272 (2007).

[26] J. Michel, J. Liu, and L. C. Kimerling, High-performance Ge-on-Si photodetectors, Nat. Photonics **4**, 527 (2010).

[27] F. Bottegoni, G. Isella, S. Cecchi, and F. Ciccacci, Spin polarized photoemission from strained Ge epilayers, Appl. Phys. Lett. **98**, 242107 (2011).

[28] F. Pezzoli, F. Bottegoni, D. Trivedi, F. Ciccacci, A. Giorgioni, P. Li, S. Cecchi, E. Grilli,Y. Song, M. Guzzi, H. Dery, and G. Isella, Optical Spin Injection and Spin Lifetime in Ge Heterostructures, Phys. Rev. Lett. **108**, 156603 (2012).

[29] E. Vitiello, M. Virgilio, A. Giorgioni, J. Frigerio, E. Gatti, S. De Cesari, E. Bonera, E. Grilli, G. Isella, and F. Pezzoli, Spin-dependent direct gap emission in tensile-strained Ge films on Si substrates, Phys. Rev. B **92**, 201203(R) (2015).

[30] N. W. Hendrickx, W. I. L. Lawrie, L. Petit, A. Sammak, G. Scappucci, and M. Veldhorst, A single-hole spin qubit, Nat. Commun. **11**, 3478 (2020).

[31] S. De Cesari, A. Balocchi, E. Vitiello, P. Jahandar, E. Grilli, T. Amand, X. Marie, M. Myronov, and F. Pezzoli, Spin-

coherent dynamics and carrier lifetime in strained $Ge_{1-x}Sn_x$ semiconductors on silicon, Phys. Rev. B **99**, 035202 (2019).
[32] P. Li and H. Dery, Spin-Orbit Symmetries of Conduction Electrons in Silicon, Phys. Rev. Lett. **107**, 107203 (2011).
[33] J-M. Tang, B. T. Collins, and M. E. Flatté, Electron spin-phonon interaction symmetries and tunable spin relaxation in silicon and germanium, Phys. Rev. B **85**, 045202 (2012).
[34] Y. Song and H. Dery, Analysis of phonon-induced spin relaxation processes in silicon, Phys. Rev. B **86**, 085201 (2012).
[35] P. Li, Y. Song, and H. Dery, Intrinsic spin lifetime of conduction electrons in germanium, Phys. Rev. B **86**, 085202 (2012).
[36] C. Guite and V. Venkataraman, Temperature dependence of spin lifetime of conduction electrons in bulk germanium, Appl. Phys. Lett. **101**, 252404 (2012).
[37] P. Li, J. Li, L. Qing, H. Dery, and I. Appelbaum, Anisotropy-Driven Spin Relaxation in Germanium, Phys. Rev. Lett. **111**, 257204 (2013).
[38] A. Giorgioni, E. Vitiello, E. Grilli, M. Guzzi, and F. Pezzoli, Valley-dependent spin polarization and long-lived electron spins in germanium, Appl. Phys. Lett. **105**, 152404 (2014).
[39] Y. Song, O. Chalaev, and H. Dery, Donor-Driven Spin Relaxation in Multivalley Semiconductors, Phys. Rev. Lett. **113**, 167201 (2014).
[40] M. Ishikawa, T. Oka, Y. Fujita, H. Sugiyama, Y. Saito, and K. Hamaya, Spin relaxation through lateral spin transport in heavily doped n-type silicon, Phys. Rev. B **95**, 115302 (2017).
[41] M. Yamada, Y. Fujita, M. Tsukahara, S. Yamada, K. Sawano, and K. Hamaya, Large impact of impurity concentration on spin transport in degenerate n-Ge, Phys. Rev. B **95**, 161304(R) (2017).
[42] O. Chalaev, Y. Song, and H. Dery, Suppressing the spin relaxation of electrons in silicon, Phys. Rev. B **95**, 035204 (2017).
[43] T. Naito, M. Yamada, S. Yamada, K. Sawano, and K. Hamaya, Suppression of Donor-Driven Spin Relaxation in Strained $Si_{0.1}Ge_{0.9}$, Phys. Rev. Applied **13**, 054025 (2020).
[44] R. People, Indirect band gap of coherently strained Ge_xSi_{1-x} bulk alloys on <001> silicon substrates, Phys. Rev. B **32**, 1405R (1985).
[45] S. Krishnamurthy, A. Sher, and A.-B. Chen, Band structures of Si_xGe_{1-x} alloys, Phys. Rev. B **33**, 1026 (1986).
[46] K. Sawano, Y. Hoshi, S. Kubo, K. Arimoto, J. Yamanaka, K. Nakagawa, K. Hamaya, M. Miyao, and Y. Shiraki, Structural and electrical properties of Ge(111) films grown on Si(111) substrates and application to Ge(111)-on-Insulator, Thin Solid Films **613**, 24 (2016).
[47] Y. Wagatsuma, M. M. Alam, K. Okada, M. Yamada, K. Hamaya, and K. Sawano, A drastic increase in critical thickness for strained SiGe by growth on mesa-patterned Ge-on-Si, Appl. Phys. Express **14**, 025502 (2021).
[48] K. Hamaya, Y. Fujita, M. Yamada, M. Kawano, S. Yamada, and K. Sawano, Spin transport and relaxation in germanium, J. Phys. D: Appl. Phys. **51**, 393001 (2018).
[49] M. Yamada, T. Ueno, T. Naito, K. Sawano, and K. Hamaya, Experimental extraction of donor-driven spin relaxation in n-type nondegenerate germanium, Phys. Rev. B **104**, 115301 (2021).
[50] J. P. Dismukes, L. Ekstrom, and R. J. Paff, Lattice Parameter and Density in Germanium-Silicon Alloys, J. Phys. Chem. **68**, 3021 (1964).
[51] Q. M. Ma and K. L. Wang, Strain-induced nonlinear energy-band splitting of $Si_{1-x}Ge_x$ alloys coherently grown on (111) and (110) oriented Ge substrates, Appl. Phys. Lett. **58**, 1184 (1991).
[52] R. Vrijen, E. Yablonovitch, K. Wang, H. W. Jiang, A. Balandin, V. Roychowdhury, T. Mor, and D. DiVincenzo, Electron-spin-resonance transistors for quantum computing in silicon-germanium heterostructures, Phys. Rev. A **62**, 012306 (2000).
[53] F. J. Jedema, H. B. Heersche, A. T. Filip, J. J. A. Baselmans, and B. J. van Wees, Electrical detection of spin precession in a metallic mesoscopic spin valve, Nature (London) **416**, 713 (2002).
[54] X. Lou, C. Adelmann, S. A. Crooker, E. S. Garlid, J. Zhang, K. S. M. Reddy, S. D. Flexner, C. J. Palmstrøm, and P. A. Crowell, Electrical detection of spin transport in lateral ferromagnet-semiconductor devices, Nat. Phys. **3**, 197 (2007).
[55] Y. Fujita, M. Yamada, M. Tsukahara, T. Naito, S. Yamada, K. Sawano, and K. Hamaya, Nonmonotonic bias dependence of local spin accumulation signals in ferromagnet/semiconductor lateral spin-valve devices, Phys. Rev. B **100**, 024431 (2019).
[56] R. Farshchi and M. Ramsteiner, Spin injection from Heusler alloys into semiconductors: A materials perspective, J. Appl. Phys. **113**, 191101 (2013).
[57] ß M. Jourdan, J. Minár, J. Braun, A. Kronenberg, S. Chadov, B. Balke, A. Gloskovskii, M. Kolbe, H.J. Elmers, G. Schönhense, H. Ebert, C. Felser, and M. Kläui, Direct observation of half-metallicity in the Heusler compound Co_2MnSi, Nat. Commun. **5**, 3974 (2014).
[58] Y. Fujita, M. Yamada, M. Tsukahara, T. Oka, S. Yamada, T. Kanashima, K. Sawano, and K. Hamaya, Spin Transport and Relaxation up to 250 K in Heavily Doped n-Type Ge Detected Using $Co_2FeAl_{0.5}Si_{0.5}$ Electrodes, Phys. Rev. Applied **8**, 014007 (2017).
[59] M. Yamada, F. Kuroda, M. Tsukahara, S. Yamada, T. Fukushima, K. Sawano, T. Oguchi, and K. Hamaya, Spin injection through energy-band symmetry matching with high spin polarization in atomically controlled ferromagnet/ferromagnet/semiconductor structures, NPG Asia Mater. **12**, 47 (2020).
[60] K. Kudo, M. Yamada, S. Honda, Y. Wagatsuma, S. Yamada, K. Sawano, and K. Hamaya, Room-temperature two-terminal magnetoresistance ratio reaching 0.1% in semiconductor-based lateral devices with $L2_1$-ordered Co_2MnSi, Appl. Phys. Lett. **118**, 162404 (2021).
[61] M. E. Flatté and J. M. Byers, Spin Diffusion in Semiconductors, Phys. Rev. Lett. **84**, 4220 (2000).
[62] I. Appelbaum, B. Huang, and D. J. Monsma, Electronic measurement and control of spin transport in silicon, Nature (London) **447**, 295 (2007).
[63] B. Huang, D. J. Monsma, and I. Appelbaum, Coherent Spin Transport through a 350 Micron Thick Silicon Wafer, Phys. Rev. Lett. **99**, 177209 (2007).

[64] T. Sasaki, Y. Ando, M. Kameno, T. Tahara, H. Koike, T. Oikawa, T. Suzuki, and M. Shiraishi, Spin Transport in Nondegenerate Si with a Spin MOSFET Structure at Room Temperature, Phys. Rev. Applied **2**, 034005 (2014).
[65] S. Sato, M. Tanaka, and R. Nakane, Spin transport in Si-based spin metal-oxide-semiconductor field-effect transistors: Spin drift effect in the inversion channel and spin relaxation in the n^+-Si source/drain regions, Phys. Rev. B **102**, 035305 (2020).
[66] R. Jansen, A. Spiesser, H. Saito, Y. Fujita, S. Yamada, K. Hamaya, and S. Yuasa, Nonlinear Electrical Spin Conversion in a Biased Ferromagnetic Tunnel Contact, Phys. Rev. Applied **10**, 064050 (2018).
[67] F. Bottegoni, C. Zucchetti, S. Dal Conte, J. Frigerio, E. Carpene, C. Vergnaud, M. Jamet, G. Isella, F. Ciccacci, G. Cerullo, and M. Finazzi, Spin-Hall Voltage over a Large Length Scale in Bulk Germanium, Phys. Rev. Lett. **118**, 167402 (2017).
[68] C. Zucchetti, F. Bottegoni, C. Vergnaud, F. Ciccacci, G. Isella, L. Ghirardini, M. Celebrano, F. Rortais, A. Ferrari, A. Marty, M. Finazzi, and M. Jamet, Imaging spin diffusion in germanium at room temperature, Phys. Rev. B **96**, 014403 (2017).
[69] Z. G. Yu and M. E. Flatté, Electric-field dependent spin diffusion and spin injection into semiconductors, Phys. Rev. B **66**, 201202(R) (2002).
[70] Z. G. Yu and M. E. Flatté, Spin diffusion and injection in semiconductor structures: Electric field effects, Phys. Rev. B **66**, 235302 (2002).
[71] A. Spiesser, Y. Fujita, H. Saito, S. Yamada, K. Hamaya, W. Mizubayashi, K. Endo, S. Yuasa, and R. Jansen, Quantification of Spin Drift in Devices with a Heavily Doped Si Channel, Phys. Rev. Applied **11**, 044020 (2019).